Int. J. Heat Mass Transfer. Vol. 26, No. 12, pp. 1791–1803, 1983
Printed in Great Britain

0017-9310/83 \$3.00 + 0.00

HEAT TRANSFER IN A TUBE BANK IN THE PRESENCE OF UPSTREAM CROSS-SECTIONAL ENLARGEMENT

E. M. SPARROW and A. A. YANEZMORENO
Department of Mechanical Engineering, University of Minnesota, Minneapolis, MN 55455, U.S.A.

(*Received* 18 *January* 1983 *and in final form* 10 *March* 1983)

Abstract—Per-tube heat transfer coefficients were determined in a tube bank in the presence of an abrupt upstream enlargement of the flow cross section. The enlargement occurred either at the inlet face of the tube bank or at the upstream end of a duct which delivered the flow to the inlet. Three different magnitudes of enlargement were investigated along with three lengths of the delivery duct. Axial pressure distributions were measured both in the tube bank and in the delivery duct, and flow visualization was performed to observe the fluid motions in the tube bank. It was found that the enlargement can give rise to appreciable increases in the tube-bank heat transfer coefficients compared with those for the no-enlargement case. The enlargement also causes an additional pressure drop which depends on the magnitude of the enlargement and, to a lesser extent, on the distance between the enlargement and the tube bank.

NOMENCLATURE

A_{min}	minimum free flow area between tubes
D	tube diameter
$\mathscr{D}$	diffusion coefficient
f	friction factor
K	per-tube mass transfer coefficient
$\dot{m}$	rate of mass transfer per unit area
$Nu_{0.7}$	Nusselt number corresponding to $Pr = 0.7$
Pr	Prandtl number
p	pressure
p_{atm}	ambient pressure
Δp_{incr}	enlargement-related incremental pressure drop
Re	Reynolds number, $\rho VD/\mu$
S	side of square duct
Sc	Schmidt number
Sh	per-tube Sherwood number, $KD/\mathscr{D}$
S_L	longitudinal pitch
S_T	transverse pitch
V	maximum velocity, $\dot{w}/\rho A_{min}$
$\dot{w}$	mass flow rate
X'	axial coordinate.

Greek symbols

μ	viscosity
ν	kinematic viscosity
ρ	air density
ρ_{nw}	naphthalene vapor density at tube surface
ρ_{nb}	naphthalene vapor density in bulk flow.

INTRODUCTION

IN TUBE-BANK crossflow heat exchangers, the crossflow fluid may be delivered to the bank via a duct whose cross section differs from the inlet-face cross section of the bank. Frequently, the area of the inlet face is substantially larger than the cross-sectional area of the duct, necessitating an enlargement either at or upstream of the inlet. Cross-sectional enlargements generally give rise to separation and accompanying flow disturbances, except for gradually tapered enlargements which are rarely encountered in heat exchanger practice because of space limitations. Most commonly, the enlargement is accomplished either abruptly or by means of a rapid taper. Depending on the distance upstream of the tube-bank inlet at which the enlargement occurs, the highly disturbed flow which it spawns may have a significant effect on the heat transfer and pressure drop characteristics of the bank.

The objective of the experiments to be reported here is to determine the heat transfer and pressure drop response of a tube bank to an abrupt enlargement of the flow cross section which occurs either upstream of or at the bank inlet. Measurements were made of the per-tube heat transfer coefficient at each tube in each successive row, starting at the first row and proceeding downstream until fully developed conditions were encountered. Pressure drops were also measured on a row-by-row basis. To supplement the heat transfer and pressure drop data, flow visualizations were performed within the tube bank to observe the paths followed by the disturbances generated by the upstream cross-sectional enlargement.

The experiments encomposed a total of nine different ducting arrangements. These included three lengths of the duct which delivers the flow to the tube-bank inlet face and three enlargements of the flow cross section. The enlargement occurs at the upstream end of the delivery duct, so that the chosen ducting arrangements position the enlargement at various distances from the tube-bank inlet face. To provide a basis for assessing the effect of the enlargement, the aforementioned experiments included the case of no enlargement. For each of the ducting arrangements, measurements were made for two Reynolds numbers which spanned an order of magnitude.

The heat transfer results will be presented in a format designed to provide an immediate indication of the effect of the enlargement. At each tube in the bank, the heat transfer coefficient in the presence of enlargement is ratioed with that for the no-enlargement case, with all other geometrical and flow parameters being held fixed. If this ratio exceeds one, then the enlargement is enhancing, while values of the ratio below one indicate degradation. The ratios which pertain to the respective tubes are inscribed on a plan-view layout of the bank,

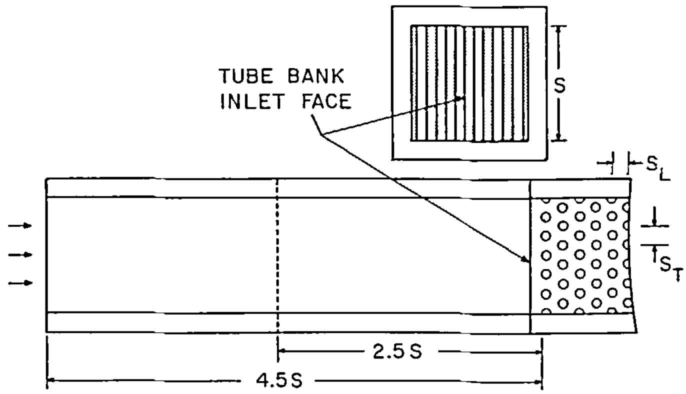

FIG. 1. Diagrams of the experimental apparatus.

thereby facilitating the identification of which portion of the bank is affected by the enlargement.

The measured pressure distributions yielded fully developed friction factors in the tube bank and incremental pressure losses associated with the presence of the enlargement. The flow visualization work was carried out using the oil-lampblack technique, and representative photographs of the flow traces are included in the paper.

The flow nonuniformity induced by an abrupt enlargement situated either at or upstream of the inlet face of a tube bank can be regarded as a maldistribution. In the heat exchanger literature, there is a keen awareness of the potential importance of maldistributed inlet flows on the performance of the exchanger, as witnessed by several papers in a recently published symposium volume [1]. However, a careful literature search did not reveal any published quantitative information on the effect of upstream cross-sectional enlargement on the heat transfer and pressure drop in a crossflow tube bank.

THE EXPERIMENTS

As noted earlier, the work included three types of experiments—heat transfer, pressure drop, and flow visualization. Both from the standpoint of higher accuracy and of experimental simplicity, mass transfer experiments offer several advantages compared with direct heat transfer experiments. In the present study, the naphthalene sublimation technique was employed to determine mass transfer coefficients which can be transformed to heat transfer coefficients by means of the analogy between the two processes.

The experimental apparatus is shown in Fig. 1. The upper part of Fig. 1 shows the inlet face of the tube bank. The cross section of the duct in which the tube bank is housed is a square of side S. The lower part of Fig. 1 is a plan view looking downward into the apparatus (as if the upper wall were removed). This diagram shows a portion of the tube bank and the entirety of the delivery duct which conveys fluid to the inlet face of the bank. The delivery duct is, in effect, an upstream extension of the duct which houses the tube bank. It is straight and of square cross section with side S.

The different lengths of the delivery duct employed during the experiments can be identified in Fig. 1. For the longest duct, the length is about $4.5S$, while the length of the intermediate duct is about $2.5S$. The shortest duct is of zero length.

The delivery duct/tube-bank system was operated in the suction mode. Air was drawn from the laboratory into the upstream end of the delivery duct or, for the delivery duct of zero length, directly into the inlet face of the tube bank. The air passed through the delivery duct and the tube bank, through a square-to-circular transition section, and then through an air-handling system consisting of flowmeters (calibrated rotameters), control valves, and blowers. The blowers were situated outside the laboratory so that their discharge, which was heated by compression and also contained naphthalene vapor, would not be recycled through the experimental apparatus.

The cross-sectional enlargements were obtained by affixing plates with different opening apertures either at the upstream end of the delivery duct or at the inlet face of the tube bank (for the delivery duct of zero length). Figures 2(a)–(c) depict the flow cross sections of the plates that were employed. Figure 2(a) shows the no-plate, no-enlargement case which serves as a baseline. Figure 2(b) shows a plate whose open area is half that of the duct, resulting in a duct-to-aperture area ratio of two. In Fig. 2(c), the duct-to-aperture area ratio is four. The plates were of 0.318 cm aluminum and were machined with a downstream-facing bevel to ensure a clean flow separation.

Attention will now be turned to the tube bank. It consisted of 15 rows of tubes deployed in a staggered,

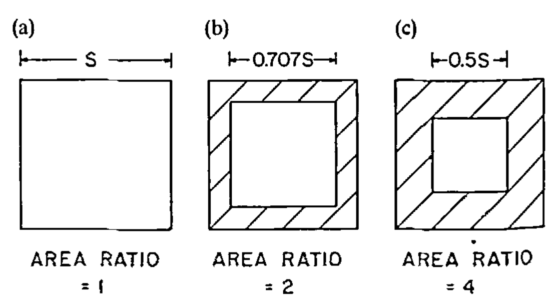

FIG. 2. Enlargement configurations.

equilateral triangular array with six tubes in each row. Such an array is characterized by $S_L = 0.866S_T$ (S_L = longitudinal pitch, S_T = transverse pitch). The selected tube diameter D and transverse spacing yielded a pitch-to-diameter ratio $S_T/D = 2$. The key dimensions of the tube bank were the tube diameter $D = 0.635$ cm and the side of the square duct which housed the bank, namely, $S = 7.62$ cm.

It may be noted that the length-to-diameter ratio of the tubes is 12, which is believed to be sufficiently large to minimize the role of end effects. Another measure to minimize end effects was the use of half tubes adjacent to the sidewalls in alternate rows as shown in Fig. 1.

In the main, the experiments were performed such that in each data run, only one of the tubes directly participated in the mass transfer process. In the various runs, the mass-transfer-active tube was deployed at different positions throughout the array. The other tubes in the array were made of steel rod stock (actually, drill rod). In a few selected data runs, as many as three rows of the array were entirely populated by mass-transfer-active tubes.

For the effective implementation of the naphthalene sublimation technique, it is necessary that there be rapid access to the test section for the installation or removal of the mass-transfer-active tubes. This is because sublimation, while much diminished, continues to occur even when there is no airflow in the test section. The required access was achieved by making the upper wall of the test section removable, with quick-acting clamps being used to lock the wall in place during the data runs.

The mass-transfer-active tubes consisted of a naphthalene coating over a cylindrical metal substrate. The surface of the substrate had been roughened by a screw-threading operation to provide better adhesion of the naphthalene. With regard to the coating process, it consisted of two distinct stages. In the first stage, the substrate was dipped repeatedly into a pool of molten naphthalene, which produced a somewhat rough, overly thick coating. The desired final dimensions and surface finish were obtained by machining the naphthalene surface on a lathe. The finished dimensions of the naphthalene-coated tubes were identical to those of the steel rods which comprised the other tubes of the array.

Each mass transfer data run consisted of two distinct parts: the equilibration period and the data run proper. During the equilibration period, the mass-transfer-active tube, situated in the test section and suitably covered to prevent sublimation, attained temperature equality with the airflow. The mass of the tube was measured prior to the data run proper. During the run, the tube was exposed to the airflow for a period of time which limited the change of thickness of the naphthalene coating to less than 0.0025 cm. At the termination of the run, the mass was measured again. After this second mass measurement, a mock data run was performed to determine the amount of sublimation that might have occurred during the installation, removal, and handling of the tube—after which the mass was once again measured. All mass measurements were performed with a Sartorius ultra-precision electronic balance capable of discriminating 10^{-5} g. The air temperature was read with an ASTM-certified thermometer with 0.1°F scale divisions.

Pressure drop measurements were made in data runs separate from the mass transfer runs. For this purpose, an axial array of pressure taps had been installed along the upper wall of the delivery duct and the test section, midway between the sidewalls. In the test section, the first tap was situated midway between the second and third rows, and subsequent taps were separated by twice the longitudinal pitch. Eight taps were installed in the delivery duct at axial stations which will be evident from the pressure drop data to be presented later. The pressure distributions were read with a Baratron capacitance-type pressure meter capable of resolving 10^{-4} mm Hg.

As noted earlier, flow visualization was carried out using the oil–lampblack technique. According to this method, a mixture of oil and lampblack powder of suitable fluidity is applied to the surface which bounds the airflow whose characteristics are to be determined. When the airflow is initiated, the mixture may move along the surface, following the paths of the fluid particles. In regions of low velocity (e.g. stagnation, separation), the mixture does not move, thereby indicating the presence of such regions. The attainment of the proper fluidity to achieve a true rendering of the flow pattern is a trial and error process. The oil–lampblack method is not very effective on vertical, inclined, or downfacing surfaces because the mixture tends to sag.

In the present study, the oil–lampblack mixture was applied to the lower wall of the test section, which had been coated with white contact paper to provide high contrast. The mixture was found to respond to the highest Reynolds numbers in the investigated range (~8400), but the forces imposed by low Reynolds number flows did not move the mixture. Because of this, all of the final visualization runs were performed at a Reynolds number of about 8400.

FLOW VISUALIZATION RESULTS

The greatest contrast between the tube-bank flow patterns which correspond to different enlargements occurs when the enlargement takes place at the inlet face of the tube bank. The oil–lampblack visualization patterns will, therefore, be presented for that case (i.e. for the delivery duct of zero length). The visualization patterns corresponding to no enlargement, two-fold enlargement, and four-fold enlargement are, respectively, shown in Figs. 3–5. In each figure, the inlet of the tube bank corresponds to the lower edge of the photograph, and the mainflow direction is from the lower edge to the upper edge.

An overview of Figs. 3–5 indicates that while the flow in the tube bank is spanwise periodic and without large-scale transverse motions when there is no enlargement (Fig. 3), these features no longer prevail in the presence of enlargement, especially in the forwardmost rows (Figs. 4 and 5). This is to be expected since the blockage

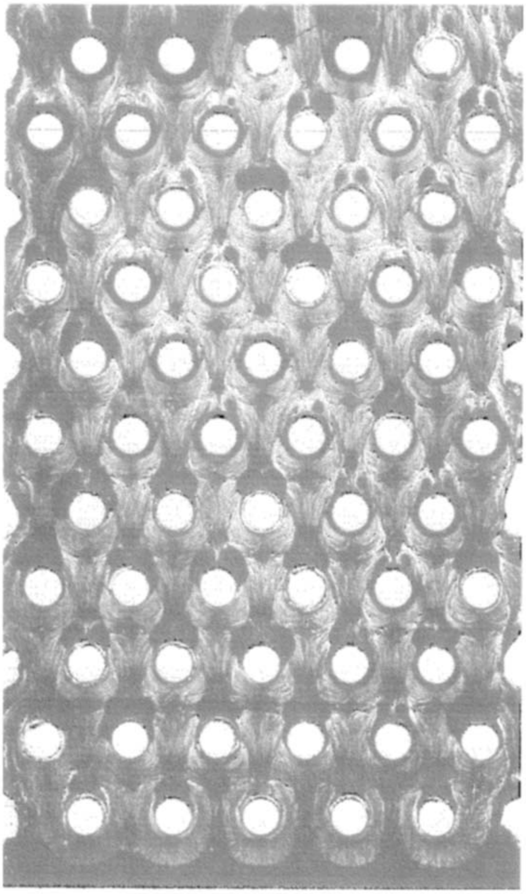

FIG. 3. Flow visualization pattern when there is no enlargement and no delivery duct.

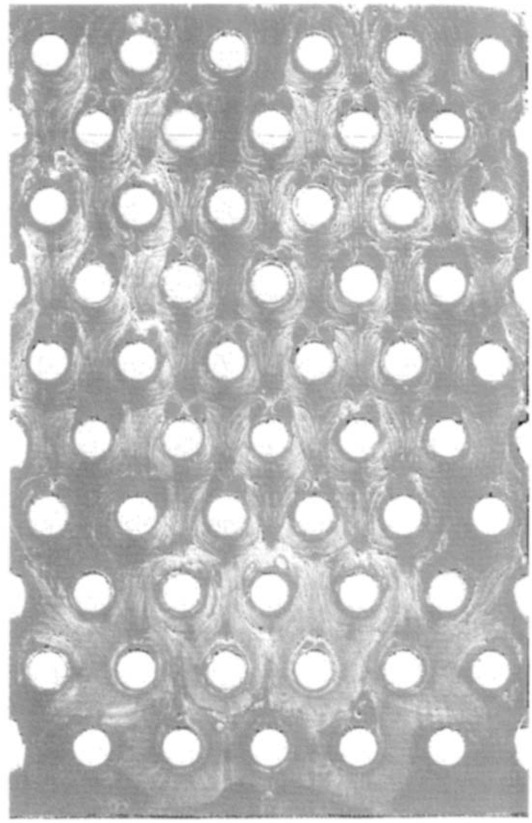

FIG. 4. Flow visualization pattern in the presence of two-fold enlargement at the tube-bank inlet.

caused by the enlargement plate [Figs. 2(b) and (c)] causes the flow to be concentrated in the central portion of the inlet cross section and, thereby, to enter the tube bank as a jet. As a consequence, the entering flow does not impinge directly on the sidewall-adjacent tubes of the forwardmost rows. The resulting lower velocities in those regions are unable to move the oil-lampblack mixture so that the initial black coating remains, as seen in the sidewall-adjacent regions in Fig. 5 and to a lesser extent in Fig. 4.

The lateral spreading of the entering jet is clearly in evidence in Fig. 4 and even more so in Fig. 5, as manifested by the tongue-like streaks which are threaded between the tubes in the first several rows. It appears that for the two-fold enlargement (Fig. 4), the flow pattern beyond the fifth row tends to coincide with that for the no-enlargement case. On the other hand, the effects of the four-fold enlargement continue to be felt farther downstream (Fig. 5). For example, in the eighth row, a tongue of fluid is seen issuing from the sidewall toward the center of the array. These lateral flows occur because the overly rapid transverse spreading of the jet gives rise to an excess of fluid near the sidewalls, and corrective motions must occur before fully developed conditions can prevail.

From a close inspection of Figs. 4 and 5, it may be conjectured that the highest heat transfer coefficients in

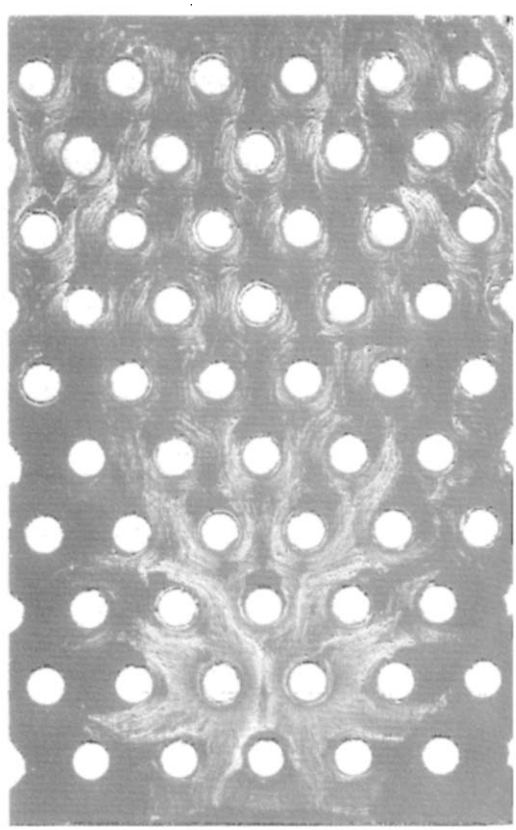

FIG. 5. Flow visualization pattern in the presence of four-fold enlargement at the tube-bank inlet.

the presence of enlargement occur in the middle of the third row. This conjecture is based on what appears to be an intense scrubbing of the duct wall in that neighborhood by the fluid. In Fig. 3 (case of zero enlargement), the flow pattern about the first row is highly distinct from that of the downstream rows, as is to be expected. The second row displays small differences from the others, but for the third row and beyond the flow pattern appears to have a fixed shape.

HEAT (MASS) TRANSFER RESULTS

The data reduction for the mass transfer work will now be briefly described, followed by the presentation and discussion of the results. In view of the analogy between the two processes, the phrases mass transfer and heat transfer will be used interchangeably during the discussion.

Data reduction

The measured per-tube change of mass during a data run, when divided by the duration of the run and the surface area of the tube, yielded the quantity $\dot{m}$. In turn, when $\dot{m}$ is divided by the concentration difference for mass transfer, $(\rho_{nw}-\rho_{nb})$, the per-tube mass transfer coefficient follows as

$$K = \dot{m}/(\rho_{nw}-\rho_{nb}). \quad (1)$$

In equation (1), ρ_{nw} is the density of the naphthalene vapor at the surface of the tube. It was evaluated from the Sogin vapor pressure–temperature relation [2] in conjunction with the perfect gas law. The quantity ρ_{nb} is the density of the naphthalene vapor in the fluid approaching the particular tube under consideration. As noted earlier, most of the data runs were made with only one mass-transfer-active tube in the array, and for that case $\rho_{nb} = 0$. In those cases where mass transfer occurred upstream of the monitored tube, then $\rho_{nb} = \dot{M}/\dot{Q}$, where $\dot{M}$ is the sum of the mass transfer rates at all the upstream tubes and $\dot{Q}$ is the volume flow rate.

In dimensionless terms, the mass transfer coefficient can be represented by the Sherwood number

$$Sh = KD/\mathscr{D} = (KD/\nu)Sc, \quad (2)$$

where, in the second form, the diffusion coefficient has been replaced by the kinematic viscosity via the Schmidt number. Note that the tube diameter D has been used as the characteristic length.

The Reynolds number will be defined in terms of the maximum velocity V and the tube diameter D, where $\rho V = \dot{w}/A_{min}$ ($\dot{w}$ is the mass flow and A_{min} is the minimum free flow area between the tubes). Therefore

$$Re = \rho VD/\mu. \quad (3)$$

The Sherwood number results obtained here correspond to a Schmidt number $Sc = 2.5$, while for heat exchanger applications, the Nusselt number for a Prandtl number $Pr = 0.7$ (airflow) is needed. According to Zukauskas [3], for flow through a tube bank $Nu \sim Pr^{0.36}$, and by analogy $Sh \sim Sc^{0.36}$. Therefore

$$Nu_{0.7} = 0.632\,Sh_{2.5}. \quad (4)$$

With the use of equation (4), the present Sherwood number results can be employed for airflow heat transfer in tube banks.

Heat (mass) transfer without enlargement

To provide a basis for evaluating the effect of upstream cross-sectional enlargement, the experimental results for the no-enlargement case will be presented first. These experiments were performed with a delivery duct of zero length as well as for delivery duct lengths equal to 2.5S and 4.5S (see Fig. 1).

The corresponding row-by-row variations of the Sherwood number are plotted in Fig. 6, for $Re = 850$ and 8400 in the lower and upper parts, respectively. To obtain the plotted values of the Sherwood number, mass transfer measurements were made at the middle three tubes in the odd rows and at the middle two tubes in the even rows, and the average was taken to be the representative value for the row. The data are interconnected by lines to provide continuity. Different ordinate scales are used for the upper and lower parts of Fig. 6, and both scales are highly expanded. To emphasize this, vertical distances corresponding to a 5% interval in the Sherwood number are shown in the figure.

Figure 6 shows the expected increase of the Sherwood number in the initial rows, as the turbulence spawned by the tubes enhances the mass transfer. At larger downstream distances, a periodic flow pattern which repeats itself in each successive row is established, so that the Sherwood number becomes a constant.

Whereas the aforementioned behavior is wholly expected, the overshoot which appears in the respective Sherwood number distributions (and which was confirmed by numerous repetitive data runs) is quite unexpected. This overshoot amounts to 2–4% of the

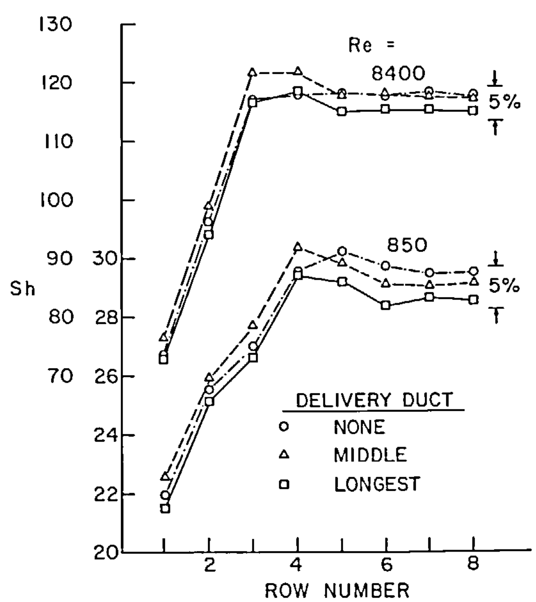

FIG. 6. Sherwood number distributions for the no-enlargement case.

respective fully developed value and is, therefore, not of major practical importance. It appears to be somewhat more strongly manifested when the delivery duct is present.

The presence of the delivery duct and its length have a modest effect (< 5%) on the Sherwood numbers in both the development and fully developed regions. Without a delivery duct, the flow tends to separate at the sharp-edged inlet face of the tube bundle. With the delivery duct in place, the flow presented to the tube bank is either a partially or fully developed channel flow. Figure 6 shows that the Sherwood numbers corresponding to the longest delivery duct are the lowest among the three cases. In the development region, the highest Sherwood numbers correspond to the medium-length delivery duct, while in the fully developed region the highest values are for the no-delivery-duct case.

The trends discussed in the foregoing paragraphs are common to both of the investigated Reynolds numbers. The thermal development of the flow is achieved somewhat more rapidly at the higher Reynolds number than at the lower Reynolds number, with fully developed conditions being attained after four to five rows.

The fully developed Sherwood numbers will now be compared with the widely quoted tube-bank heat transfer correlation of Zukauskas [3]. For this purpose, for each Reynolds number, the fully developed Sherwood numbers for the three delivery-duct configurations were averaged, yielding $Sh = 29.3$ and 117.1, respectively for $Re = 850$ and 8400. The corresponding Sherwood numbers from the Zukauskas correlation are 28.7 and 113.3. The deviations are in the 2–3% range, which can be regarded as very good agreement.

The results which have been presented in the preceding portion of this section were obtained from experiments in which mass transfer occurred at only one tube in the array. Attention will now be turned to results of experiments in which there were many mass-transfer-active tubes in the array. For these experiments, all of the whole tubes in rows four, five, and six—a total of 17 tubes—were naphthalene coated. The wall-adjacent half tubes in the fifth row could not be coated, but this limitation did not affect the Sherwood numbers, which were purposefully evaluated at the tubes in the middle of the sixth row. The tubes in the other rows were metallic. Although it would have been desirable to have populated additional rows with mass-transfer-active tubes, it was not possible to execute the experiment with any more than the 17 active tubes that were employed.

For both $Re = 850$ and 8400, four data runs were carried out with the multi-active-tube arrangement. The Sherwood numbers for each Reynolds number were averaged and then compared with the corresponding values obtained from the experiments performed with a single mass-transfer-active tube. For $Re = 8400$, the Sherwood numbers for the two cases were virtually identical, while for $Re = 850$, the Sherwood number for the multi-active case was 2.8% above that for the single-active case. This finding lends support to the use of results from single-active-tube experiments for predicting the performance of fully active arrays.

Heat (mass) transfer with enlargement

The per-tube heat (mass) transfer results in the presence of upstream cross-sectional enlargement are presented in Figs. 7–10. These figures convey a great deal of information and, before discussing the substance of the results, it is appropriate to describe the format, which is common to all of them.

Each of Figs. 7–10 corresponds to a given enlargement and a given Reynolds number. Figures 7 and 8 are both for a four-fold enlargement and, respectively, for $Re = 850$ and 8400. Similarly, Figs. 9 and 10 are both for a two-fold enlargement, with $Re = 850$ and 8400, respectively. An indication of the extent of the enlargement is shown by the dashed lines at the bottom of each figure. The direction of the mainflow is from the bottom to the top of the figure. To facilitate the discussion of the format, attention may be focused on any one among Figs. 7–10, say, Fig. 7.

Figure 7 is a plan view of the array, and numbers are inscribed adjacent to each tube. There are, in fact, two sets of numerical results that are presented, one set being a Sherwood number ratio and the other set being the Sherwood number itself. The values of the Sherwood number ratio are inscribed in the LHS of the array while the Sherwood numbers are inscribed in the RHS. The two halves of the array may be thought of as being separated by a symmetry line which runs parallel to the two sidewalls, midway between them. Because the area enlargement plates were centered in the cross section (Fig. 2), symmetry prevailed both with and without enlargement. Any slight data scatter at symmetric tube locations was averaged out, and the thus-obtained average values are reported.

The Sherwood number ratios that appear in the LHS will now be explained. Adjacent to each tube, three numbers are generally inscribed (at downstream rows, only one or two numbers may appear). The uppermost of the three numbers pertains to the case where the enlargement occurs at the inlet face of the tube bundle (i.e. no delivery duct). Similarly, the middle and lowermost numbers correspond, respectively, to the cases where the enlargement occurs at the upstream end of the intermediate and longest delivery ducts (Fig. 1).

Each number represents the ratio

$$\frac{Sh\text{ (with enlargement)}}{Sh\text{ (without enlargement)}}, \tag{5}$$

where both the numerator and denominator of (5) correspond to the same tube position, the same delivery duct length, and the same Reynolds number. The Sh values for the denominator are those of Fig. 6. Note that for the trio of numbers inscribed adjacent to a particular tube location, the denominators are not quite equal.

The Sherwood number ratios are listed to the left of the tube location to which they pertain. The listing of the ratios is continued in the downstream direction

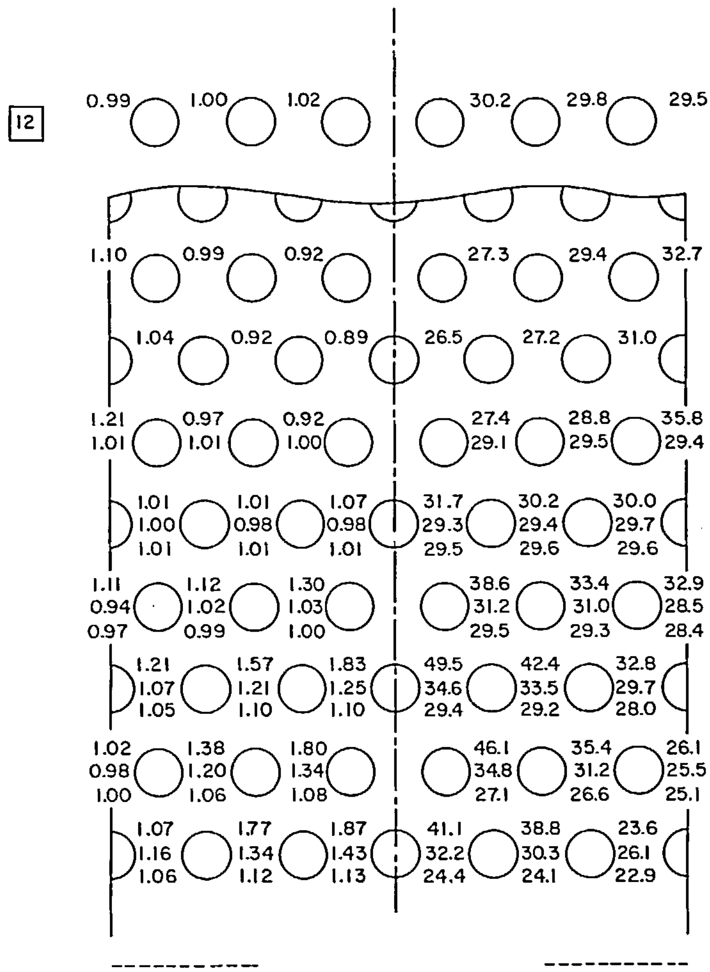

FIG. 7. Sherwood numbers and Sherwood number ratios for a four-fold enlargement and $Re = 850$.

until they are more or less equal to unity and then is terminated. The attainment of this condition is more rapid when the delivery duct is in place, and this explains the early termination of the listings for those cases.

The format of the Sherwood number listing in the RHS will now be illuminated. The numbers that appear to the right of each tube location are the Sherwood numbers for that location. For each set of numbers, the upper, middle, and lower entries correspond, respectively, to enlargement at the tube bundle inlet face and at the upstream end of the intermediate and longest delivery ducts. The row-by-row listing for each delivery duct is continued downstream until a fully developed value is obtained, at which point the listing is terminated.

The reason for presenting both Sherwood number ratios and Sherwood numbers is that each conveys a different type of information. The Sherwood number ratios provide a direct measure of whether enlargement enhances or degrades the per-tube Sherwood number, with ratios larger than one indicating enhancement and ratios below one indicating degradation. However, the largest ratios do not correspond to the largest Sherwood numbers nor do the smallest ratios correspond to the smallest Sherwood numbers. It is for this reason that the actual Sherwood numbers are also listed.

The discussion will now be directed to the trends in the Sherwood number ratio. From an overview of Figs. 7–10, it is seen that the ratios in excess of one far outweigh the ratios that are less than one. Even among the ratios whose values are less than one, most are only a few percent below, and only two values are less than 0.9 (0.86 and 0.89, respectively). Therefore, the presence of the enlargement enhances the tube bundle heat transfer. Furthermore, the larger the enlargement ratio, the greater is the enhancement, as can be seen by comparing Figs. 7 and 8 with Figs. 9 and 10. The extent of the enhancement is also strongly influenced by the location of the enlargement, with greater enhancements being encountered when the enlargement occurs closer to the bundle inlet.

On the other hand, the closer the enlargement to the bundle inlet and the greater the enlargement ratio, the larger is the overall nonuniformity of the Sherwood number ratio in a given row. These intra-row nonuniformities result because the fluid flow entering

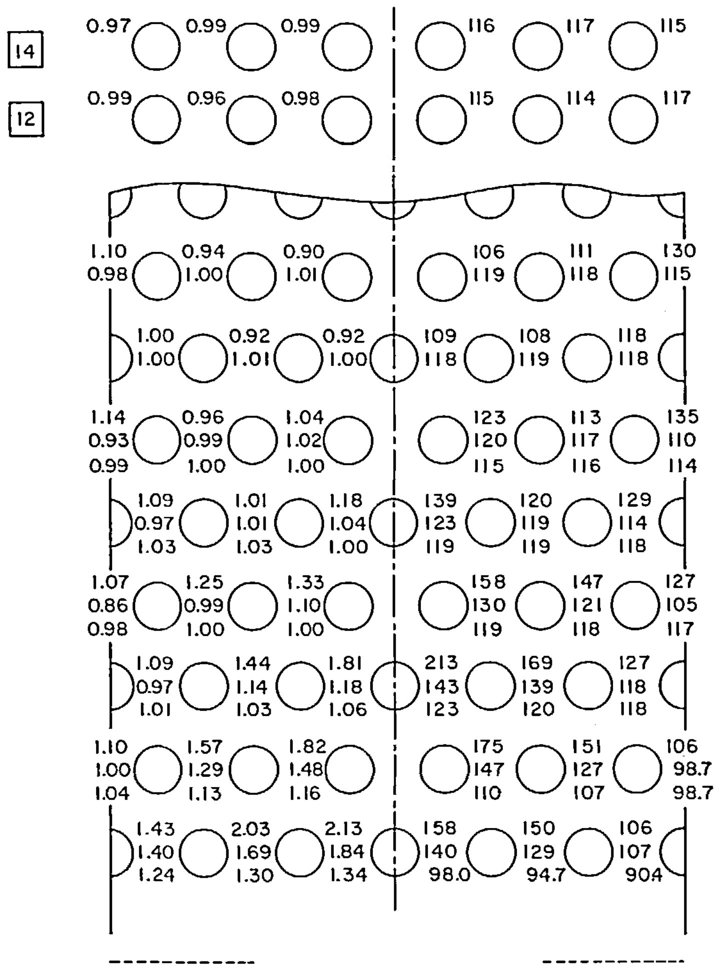

FIG. 8. Sherwood numbers and Sherwood number ratios for a four-fold enlargement and $Re = 8400$.

the tube bundle is concentrated in the central region of the inlet cross section. Therefore, in the initial rows of the bundle, lower values of the Sherwood number ratio are encountered adjacent to the sidewalls. These nonuniformities disappear with increasing downstream distance.

However, in the extreme case when the largest enlargement ratio occurs at the bundle inlet face, a secondary intra-row nonuniformity appears downstream, whereby the highest Sherwood number ratio in the row occurs adjacent to the sidewalls (Figs. 7 and 8). This behavior is consistent with the findings of the flow visualization studies, where it was noted that overly rapid transverse spreading of the flow in the initial rows gives rise to an excess of fluid adjacent to the sidewalls in the later rows. The secondary intra-row nonuniformity dies away at sufficient downstream distances.

The greatest enhancements occur in the first row of the tube bundle. The extent of the enhancement encountered there increases somewhat with the Reynolds number and markedly with the enlargement ratio and with closer proximity of the enlargement to the bundle inlet. It is also interesting to observe that for the greatest enlargement ratio and closest proximity, concerns about a possible 'dead-water', degraded-Sherwood-number zone directly behind the enlargement step did not materialize. In Fig. 8, first-row enhancements that exceed a factor of two are in evidence, and enhancements almost as large occur in the first three rows in both Figs. 7 and 8.

Significant effects of the enlargement ($\geq 10\%$) persist to the eighth row for the four-fold enlargement positioned at the inlet face of the bundle (Figs. 7 and 8). This deep penetration into the bundle is associated with the previously discussed secondary fluid flow nonuniformity. For the inlet-positioned two-fold enlargement, 10% effects are felt through the fourth row (Figs. 9 and 10).

When the enlargement occurs at the upstream end of the delivery duct, its effect does not penetrate as far into the bundle as when the enlargement occurs at the bundle inlet. For example, in the case of the longest delivery duct and a four-fold enlargement, the effect persists to the third row for $Re = 850$ (Fig. 7) and only to the second row for $Re = 8400$ (Fig. 8). Even shorter penetrations are in evidence for the two-fold enlargements (Figs. 9 and 10).

The row-by-row progression of the Sherwood

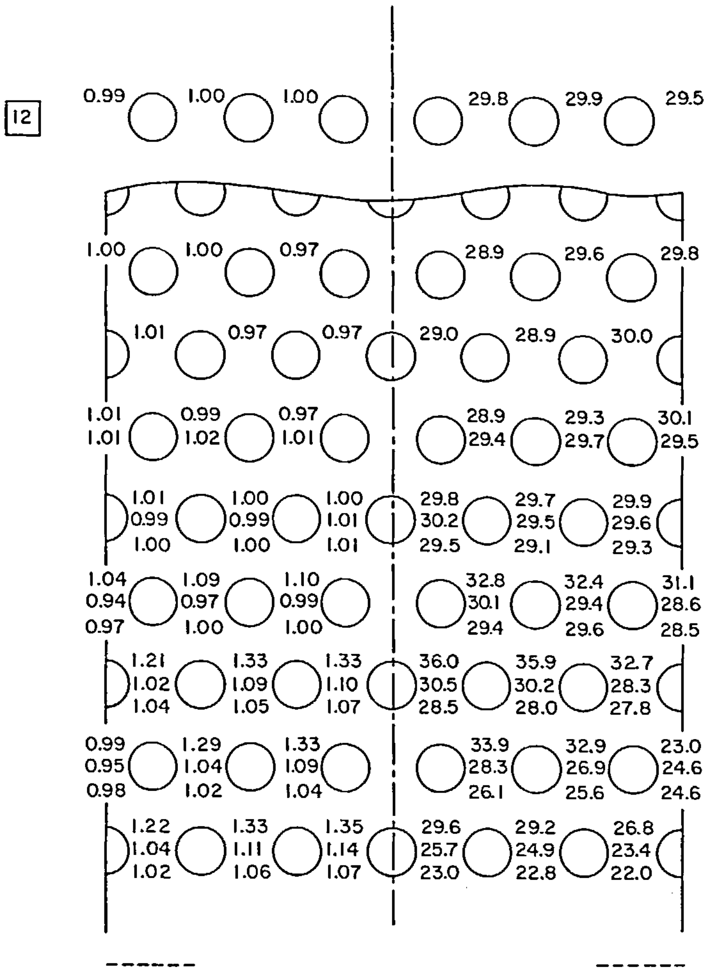

FIG. 9. Sherwood numbers and Sherwood number ratios for a two-fold enlargement and $Re = 850$.

number ratios toward a downstream value of unity is not necessarily monotonic. This is because both the numerator and denominator Sherwood numbers which comprise the ratio may vary nonmonotonically from row to row. In particular, in connection with the denominator values, there is an overshoot which was identified in connection with Fig. 6. The nonmonotonic behavior of the numerator will be discussed shortly.

Attention will now be turned to the Sherwood number values listed in the RHS of Figs. 7–10. To identify the main trends, it is useful to focus on a given enlargement ratio and enlargement positioning and to follow the Sherwood number from row to row. For the four-fold enlargement at the closest position, the Sherwood number increases from the first to the third rows, at which point it attains a maximum and then drops off very sharply, followed by a more gradual decline. Farther downstream, localized increases occur adjacent to the sidewalls as a result of the previously mentioned secondary fluid flow nonuniformity.

For the same enlargement ratio but with the enlargement at the intermediate position, the maximum is now shared by the second and third rows and is also less lofty. With the enlargement at the position farthest upstream of the bundle inlet, the Sherwood number varies monotonically from row to row for $Re = 850$ but displays a slight maximum for $Re = 8400$. The localized Sherwood number increases in the downstream part of the bundle, which were observed for the close-positioned enlargement, do not occur when the enlargement is positioned upstream of the bundle inlet.

For the two-fold enlargement and $Re = 850$ (Fig. 9), an unambiguous maximum occurs (in the third row) only at the closest positioning of the enlargement. When $Re = 8400$ (Fig. 10), maxima (also in the third row) are in evidence for the first two enlargement positions, but to a lesser extent as the position moves upstream of the inlet.

It is relevant to note that the flow visualization in Figs. 4 and 5, foretold the presence of the third-row maxima.

By examining the trio of Sherwood numbers adjacent to each tube location, the effect of the delivery duct length can be identified. The variations among the numerical values which constitute a given trio are, of course, greatest in the initial rows. These variations are impressively large in the presence of the four-fold

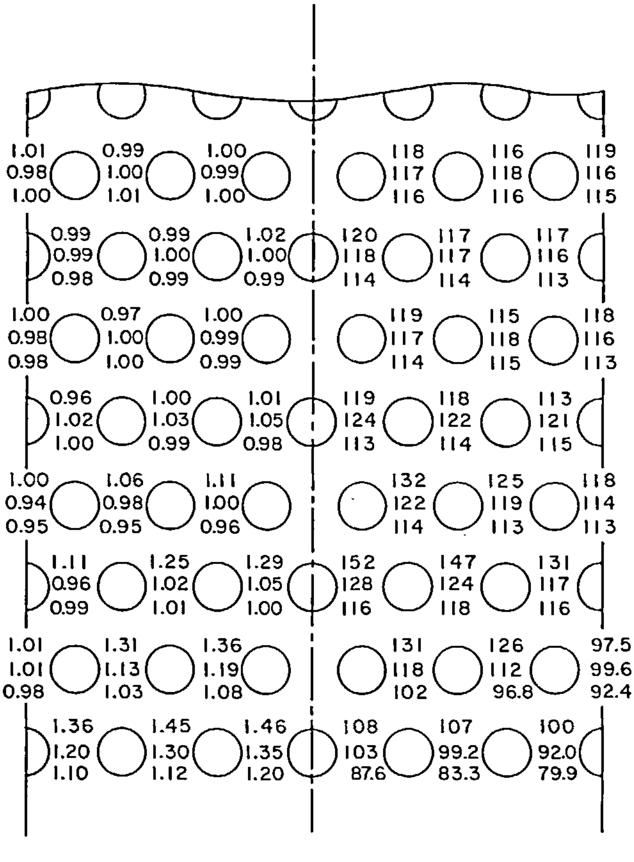

Fig. 10. Sherwood numbers and Sherwood number ratios for a two-fold enlargement and $Re = 8400$.

enlargement but are more moderate for the two-fold enlargement.

PRESSURE DROP RESULTS

As was noted earlier, taps had been installed along the upper wall of the delivery duct and the test section to enable the measurement of the axial pressure distributions. For each case (i.e. given delivery duct length, enlargement ratio, and Reynolds number), the measurements yielded the distribution of $(p_{atm}-p)$, where p is the local pressure at any tap location and p_{atm} is the ambient pressure in the laboratory from which the air was drawn. To obtain a dimensionless representation, it is appropriate to normalize the aforementioned pressure difference by a representative velocity head $\frac{1}{2}\rho V^2$ which is a constant for each case. For this purpose, ρV^2 was evaluated as

$$\rho V^2 = \dot{w}^2/\rho A_{min}^2, \qquad (6)$$

where $\dot{w}$ and A_{min} are defined in the text just prior to equation (3), and ρ is the average density in the test section (evaluated at the seventh row).

Figures showing the axial distributions of $(p_{atm}-p)/\frac{1}{2}\rho V^2$ are available for each delivery duct length. However, to conserve space, only the figure for the longest delivery duct need be presented here. As will be shown shortly, this figure can be used to describe the characteristics of the pressure distributions for the other delivery ducts.

The pressure distributions are presented in Fig. 11. The data shown there, all for the longest delivery duct, are parameterized by the enlargement ratio (1, 2, 4) and by the Reynolds number (850, 8400). On the abscissa, $X = 0$ corresponds to the inlet face of the tube bundle. Axial stations to the left of $X = 0$ are situated in the delivery duct. For those stations, the abscissa variable is X/S (S is the side of the square delivery duct). The tube bundle is situated to the right of $X = 0$, and here the row number is used as the abscissa variable (the markers for the row numbers are positioned at the centers of the tubes). Owing to the fact that $(p_{atm}-p)$ appears on the ordinate, an increasing trend in the data indicates a dropping pressure, while a decreasing trend in the data indicates a pressure rise.

Attention is first turned to the pressure distributions in the tube bundle. As noted earlier, the first tap is situated midway between the second and third rows, and subsequent taps are spaced two rows apart. It is seen that for each case, the data fall on a straight line, which suggests that fully developed conditions prevail at the third and all subsequent rows. This development is slightly more rapid than that for the development of the tube-bundle Sherwood number distributions in the presence of the longest delivery duct. This finding is consistent with the fact that the pressure distribution develops more rapidly than the velocity field. The slopes of the three lines for $Re = 850$ are nearly the same, and similarly for the three lines for $Re = 8400$. This characteristic will be employed shortly in the determination of quantitative pressure-related parameters.

Next, turning to the delivery duct, it may be noted that the flow separation which takes place at the upstream end of the duct has a marked effect on the pressure distribution, especially at larger enlargement ratios. For the four-fold enlargement, the pressure drop (shown as a rise in the figure) between the first and second stations is due to the acceleration of the fluid as it pinches together downstream of the enlargement plate (i.e. *vena contracta* effect). Subsequently, there is a pressure rise (a decrease in the figure) associated with the velocity decrease which accompanies the expansion of the fluid into the enlarged cross section. The pressure rise continues to occur up to the last pressure tap in the delivery duct, indicating that the expansion has not been completed at that station.

For the two-fold enlargement, the aforementioned *vena contracta* effect is no longer in evidence, and the first few taps display a rising pressure. Near the downstream end of the delivery duct, the pressure appears to be independent of X. Since the friction-related pressure drop is too small to be seen in the scale of the figure, the apparent pressure uniformity indicates that the inertia-related effects spawned by the enlargement have died away, although it is improbable that the flow is fully developed.

Even in the absence of an enlargement plate at the upstream end of the delivery duct, there is a small zone of separation due to the sharp-edged nature of the inlet. The pressure recovery downstream of the separated region is reflected by the first and second data points for the zero-enlargement case. The subsequent data points are essentially at uniform pressure, reflecting the virtually imperceptible friction-induced pressure drop. Although not completely fully developed, the flow arriving at the inlet face of the tube bundle should have experienced substantial development.

In the intermediate-length delivery duct, the measured pressure distribution for each case is essentially identical to the first four data points in the corresponding delivery-duct pressure distribution of Fig. 11. Furthermore, the tube-bundle pressure distributions are very similar to those of Fig. 11. For the case of no delivery duct, the measured tube-bundle pressure distributions are also similar to the distributions of Fig. 11, except that the data from the first tap do not lie on the straight lines which pass through the data from the other taps.

The presence of the enlargement gives rise to an additional pressure drop relative to the no-enlargement case. For the longest delivery duct, the enlargement-induced incremental pressure drops Δp_{incr} can be read from Fig. 11 as the vertical distances between the straight lines appearing on the RHS. For example, for $Re = 850$ and a four-fold enlargement, $\Delta p_{\text{incr}}/\frac{1}{2}\rho V^2$ is read between the uppermost and lowermost straight lines that pass through the circle data symbols. Values read in this way from Fig. 11 and from similar figures for the intermediate- and no-delivery-duct cases are listed in Table 1.

Table 1 shows that the incremental pressure drop ranges from 7.5 to 12 velocity heads for the four-fold enlargement and from 1.3 to 2.5 heads for the two-fold enlargement. There is no appreciable difference between the results for the longest and intermediate delivery ducts, but there is a significant increase in the pressure loss when the enlargement occurs at the inlet face of the tube bundle (i.e. no delivery duct). Table 1 also shows that the smaller the Reynolds number, the larger is the value of $\Delta p_{\text{incr}}/\frac{1}{2}\rho V^2$.

Fully developed friction factors in the tube bundle

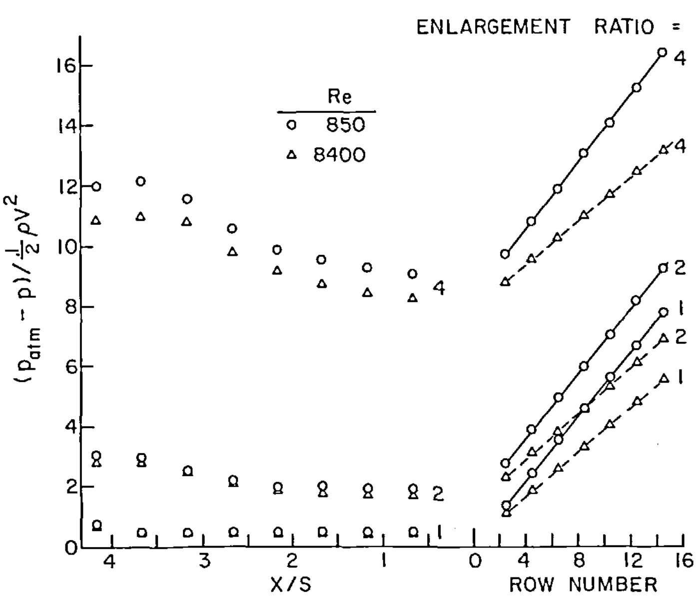

FIG. 11. Pressure distributions in the longest delivery duct and in the tube bank.

Table 1. Incremental pressure drop $\Delta p_{incr}/\frac{1}{2}\rho V^2$ due to enlargement

		Delivery duct		
Re	*Area ratio*	Longest	Middle	None
850	2	1.4	1.5	2.5
850	4	8.4	8.9	11.9
8400	2	1.3	1.3	1.8
8400	4	7.6	7.5	9.2

can be determined from least-squares straight lines fitted through the pressure distributions. If $(-dp/dN)$ represents the pressure drop per row, then the friction factor was evaluated from

$$f = (-dp/dN)/\tfrac{1}{2}\rho V^2. \quad (7)$$

For a given Reynolds number, the fully developed friction factor was found to be only slightly affected by the delivery duct or by the enlargement. These variations were averaged out, yielding $f = 0.56$ and 0.36, respectively for $Re = 850$ and 8400.

CONCLUDING REMARKS

The results presented here have shown that the presence of an abrupt cross-sectional enlargement upstream of a tube bank can give rise to appreciable increases in the heat transfer coefficient, with the no-enlargement case. Thus, the use of heat transfer information from the literature (presumably for no enlargement) to design a tube bank with upstream enlargement is conservative. On the other hand, the enlargement causes an additional pressure loss as listed in Table 1, and these losses should be included in the fluid flow design calculations.

Acknowledgment—The research reported here was performed under the auspices of the Office of Naval Research.

REFERENCES

1. S. Kakac, R. K. Shah and A. E. Bergles, *Low Reynolds Number Flow Heat Exchangers*. Hemisphere, Washington, DC (1982).
2. H. H. Sogin, Sublimation from discs to air streams flowing normal to their surfaces, *Trans. Am. Soc. Mech. Engrs.* 80, 61–71 (1958).
3. A. A. Zukauskas, Heat transfer from tubes in crossflow, in *Advances in Heat Transfer*, Vol. 8. Academic Press, New York (1972).

TRANSFERT THERMIQUE DANS UN FAISCEAU DE TUBES EN PRESENCE, EN AMONT, D'UN ELARGISSEMENT DE SECTION DROITE DU CANAL

Résumé—Les coefficients de transfert thermique rapportés au tube sont déterminés dans un faisceau de tubes en présence d'un élargissement abrupt de courant en amont. L'élargissement est situé soit à l'entrée du faisceau soit à l'extrémité d'entrée du canal qui limite l'écoulement. Trois types d'élargissement ont été étudiés avec trois longueurs du canal d'alimentation. Les distributions axiales de pression sont mesurées à la fois dans le faisceau de tubes et dans le canal et une visualisation de l'écoulement est effectuée pour observer les mouvements du fluide dans le faisceau de tubes. On trouve que l'élargissement peut créer un accroissement sensible des coefficients de transfert thermique dans le faisceau en comparaison avec le cas sans élargissement. L'élargissement provoque aussi une chute de pression additionnelle qui dépend de l'importance de l'élargissement et, à un moindre degré, de la distance entre l'élargissement et le faisceau de tubes.

WÄRMEÜBERTRAGUNG IN EINEM ROHRBÜNDEL MIT EINER STROMAUFWÄRTS GELEGENEN QUERSCHNITTSERWEITERUNG

Zusammenfassung—In einem Rohrbündel, das hinter einer plötzlichen Querschnittserweiterung angeordnet ist, wurden die Wärmeübergangskoeffizienten bestimmt. Die Erweiterung befindet sich entweder direkt am Eintrittsquerschnitt des Rohrbündels oder am Eintritt in einen vorgesetzten Zuleitungskanal. Drei unterschiedliche Querschnittserweiterungen und drei verschiedene Längen des Zuleitungskanals wurden untersucht. Im Rohrbündel und im Zuleitungskanal wurde die Druckverteilung in axialer Richtung gemessen und durch Sichtbarmachen der Strömung die Fluidbewegung im Rohrbündel beobachtet. Es ergab sich, daß der Wärmeübergang im Rohrbündel durch die Querschnittserweiterung erheblich vergrößert werden kann. Die Erweiterung des Querschnitts verursacht aber auch einen zusätzlichen Druckabfall, der vom Ausmaß der Vergrößerung abhängt und, etwas weniger stark, vom Abstand zwischen der Erweiterung und dem Rohrbündel.

ТЕПЛОПЕРЕНОС В ПУЧКЕ ТРУБ ПРИ РАСШИРЕНИИ ПОПЕРЕЧНОГО СЕЧЕНИЯ ПОТОКА ПЕРЕД ПУЧКОМ

Аннотация—Проведено определение коэффициентов теплопереноса для каждой трубы в пучке при наличии перед ним внезапного расширения поперечного сечения потока. Расширение происходит или же на передней торцевой поверхности пучка или же на выходе из трубопровода, по которому подается поток. Исследовалось три различных значения расширения сечения при трех различных значениях длины трубопровода. Аксиальные распределения давления измерялись как в пучке, так и в трубопроводе, а для определения характера обтекания труб в пучке производилась визуализация потока. Показано, что расширение сечения потока может приводить к существенному увеличению коэффициентов теплопереноса пучка по сравнению со случаем без расширения. Кроме того, при расширении наблюдается дополнительный перепад давления, который зависит от величины расширения и, в меньшей степени, от расстояния между плоскостью расширения и пучком труб.